An Agile Multi-Node Multi-Antenna Wireless Channel Sounding System

Assefa, Dereje; Rodriguez, Ignacio; Berardinelli, Gilberto; Tavares, Fernando Menezes Leitão; Sørensen, Troels Bundgaard; Hansen, Thomas Lundgaard; Mogensen, Preben Elgaard

Published in:
IEEE Access

DOI (link to publication from Publisher):
10.1109/ACCESS.2019.2895412

Publication date:
2019

Document Version
Publisher's PDF, also known as Version of record

IEEE Access
Multidisciplinary | Rapid Review | Open Access Journal

Received November 5, 2018, accepted January 3, 2019, date of publication January 31, 2019, date of current version February 14, 2019.

Digital Object Identifier 10.1109/ACCESS.2019.2895412

An Agile Multi-Node Multi-Antenna Wireless Channel Sounding System

DEREJE ASSEFA WASSIE[1], IGNACIO RODRIGUEZ[1], GILBERTO BERARDINELLI[1], FERNANDO M. L. TAVARES[1], TROELS B. SØRENSEN[1], THOMAS L. HANSEN[1], AND PREBEN MOGENSEN[1,2]

[1]Wireless Communication Networks Section, Department of Electronic Systems, Aalborg University, 9220 Aalborg, Denmark
[2]Nokia Bell Labs, 9220 Aalborg, Denmark

Corresponding author: Gilberto Berardinelli (gb@es.aau.dk)

ABSTRACT The upcoming fifth-generation wireless technology application areas bring new communication performance requirements, mainly in terms of reliability and latency, but also in terms of radio planning, where the further detailed characterization of the wireless channel is needed. To address these demands, we developed an agile multi-node multi-antenna wireless channel sounding system, using multiple software-defined radio devices. The system consists of 12 testbed nodes which are controlled from a centralized testbed server. Each node features a control host computer and two multi-antenna universal software radio peripheral boards. By managing the transmission and reception of reference signals among all the distributed testbed nodes, the system can measure the channel conditions of all multiple independent radio links. At the same time, the distributed architecture of the testbed allows a large number of spatially distributed locations to be covered with only a few redeployments of the testbed nodes. As a consequence of this, the system favors the collection of a large number of distributed channel samples with limited effort within a short dedicated measurement time. In this paper, we detail the general testbed design considerations, along with the specific sounding signal processing implementations. As further support to the system design, we also include the results from different verification and calibration tests, as well as a real measurement application example.

INDEX TERMS Channel sounding, multi-antenna, multi-node, SDR, USRP.

I. INTRODUCTION

In the last three decades, wireless communication systems have evolved from the 1^{st} generation to the 4^{th} generation, with the primary aim of improving user cellular broadband services. The upcoming 5^{th} generation (5G) systems are also expected to enhance the wireless connection capabilities towards connecting things. Wireless connected things in the context of 5G are envisioned to be employed in new application areas, e.g., smart factories, smart grids, and health-care, as prominent examples. Apart from new communication requirements in terms of latency and reliability, these new areas entail new and unconventional deployment scenarios [1]. These scenarios, including, for example, deployments in deep underground, inside factory clutter, at low antenna height or at different frequency bands, may be quite different from the typical urban/rural outdoor and indoor cases [2]. As a result, different propagation conditions may apply, which brings the need for further detailed characterization of the wireless channel. For example, with 5G applied to automation in the factories of the future (Industry 4.0) [3], [4], a process controller may need to communicate simultaneously, and wirelessly with sensors and actuators, which are deployed in different locations, in a very robust and reliable manner. Therefore, not only the outage due to channel fading on the single link becomes of interest, but, also the outage of the composite channel considering multiple simultaneous links.

Known sounding approaches for characterizing the radio channel distortion (i.e., channel fading) [5] include direct radio-frequency pulse excitation, transmission of multi-tone reference signals, frequency sweeping, or transmission of a spread spectrum waveform with a sliding correlator at the receiver. The implementations of such systems have typically been built using specialized and/or very expensive equipment (e.g., spectrum analyzer, wideband signal generator, vector network analyzer, etc.) [6]–[9]. As an alternative, there have been other more cost-effective and flexible

The associate editor coordinating the review of this manuscript and approving it for publication was Rui Wang.

TABLE 1. SDR USRP-based channel sounding systems for below 6 GHz.

Reference	Sounding Method	Software Platform	Carrier Frequency	Clock Synchronization	Main Specific Features
[11]	spread-spectrum sliding correlation	GNU Radio	2.4-2.5 GHz 4.9-5.9 GHz	via RF cable	4 MHz RF bandwidth, single TX and RX, covers short distances.
[12]	multi-tone, reference signal-based	GNU Radio	2.4 GHz	not specified	RX estimates channel impulse response of a packet transmitted from a IEEE 802.11b access point with a time resolution of 125 ns.
[13]	frequency sweep	LabVIEW	not specified	via HW reference time	20 MHz RF bandwidth, single TX and RX.
[14]	sliding correlation & multi-tone	GNU Radio	1 MHz-6 GHz	via GPS	8-20 MHz RF bandwidth, 6 TXs and single RX.
[15]	multi-tone, OFDM-based	not specified	5.9 GHz	via GPS-disciplined rubidium clocks	Single TX and RX, support of up to 4x4 MIMO with 15 MHz RF bandwidth.
[16]	multi-tone, reference signal-based	GNU Radio	2.4-2.5 GHz	not specified	2 MHz RF bandwidth, estimation based on IEEE 802.11a waveform.
[17]	multi-tone, OFDM-based	not specified	1.2-6 GHz	not specified	Built from 2 X310 USRPs which support 20-100 MHz RF bandwidth.
[18]	correlation-based	LabVIEW & GNU Radio	5.8 GHz	not specified	2 nodes, measures fast channel variations with the support of 93 MHz RF bandwidth.

implementations which are based on the software defined radio (SDR) concept. With SDR, the baseband signal processing of the radio frequency (RF) signals is handled by software, rather than using specialized hardware. This offers a high degree of flexibility, and the prominent benefit of ease of reconfigurability and rapid prototyping. On the downside, compared to the specialized systems, SDR systems are limited, among other aspects, in frequency range, transmission bandwidth, and receiver dynamic range.

A large number of channel sounding systems have been reported in [10]. By design, each of the systems considers a very specific implementation and frequency range of operation. Table 1 presents a list of some SDR-based channel sounder systems presented in the recent literature [11]–[18]. The focus here is on channel sounder systems operating at frequency below 6 GHz, since this is the spectrum range of interest for our design. The considered designs are built on universal software radio peripheral (USRP) platforms [19]. For comparison, Table 1 includes sounding method, carrier frequency, transmitter (TX) - receiver (RX) synchronization method, and main specific measurement features. As it is described in the table, most of the designs support limited frequency ranges and low transmission bandwidth. Also, they are built with a relatively low number of transmitter and receiver nodes, if not only one of each. This limits, practically, the ability to characterize a large number of links, as required for proper statistical outage characterization, due to the needed number of laborsome redeployments. Similarly, the limited number of nodes also restricts the ability to characterize the composite radio channel, considering multiple simultaneous links, due to the inevitable change from redeploying nodes.

The design goal of the testbed presented in this paper is to overcome some of these limitations, by applying a distributed multi-node multi-antenna approach. The testbed consists of 12 testbed transceiver nodes equipped with 4 antennas, and uses a multi-tone channel sounding method to measure, all the 2112 independent radio links between the nodes, within a single measurement snapshot. The radio channel sounder is developed using the NI LabVIEW communications system design suite [20], and NI USRP-R2953 boards [21], supporting a wide range of carrier frequencies, spanning from 1.2 to 6 GHz, with up to 40 MHz of RF channel bandwidth.

As compared to the existing systems, the multi-node and multi-antenna sounder system presented in this paper has a distinctive feature towards measuring multiple channel links, thus generating not only more samples, but also a consistent set of samples for statistical channel characterization. Also, by virtue of the employed SDR devices, the system supports larger frequency spans and transmission bandwidth as compared to most of the existing systems. However, achieving accurate channel measurement across multiple links using the SDR devices presents several challenges. First, typically, SDR devices have somewhat limited specifications in relation to the requirements for channel sounding, particularly concerning phase noise, long-term stability, and dynamic range. Second, the presence of multiple nodes arises challenges towards managing and automating the system. Therefore, this paper introduces the overall system design as well as the specific implementation parameters, which have been carefully selected to overcome these challenges. It should be noted that, in any case, the overall design principles of the sounder are extensible to other specific implementations based on devices with different capabilities. Further, this paper shows how statistical radio channel characterization can be enhanced when using the multi-node sounding system in conjunction with appropriate measurement procedures.

The paper is organized as follows. In Section II, we describe the architecture and design of the wireless channel sounding system. In Section III, we detail the reasoning behind the selection of each of the specific implementation parameters. Section IV presents the results from the verification and calibration tests. In Section V, we illustrate the advantages of using our multi-node setup in actual field tests. Finally, the conclusions and future work are presented in Section VI.

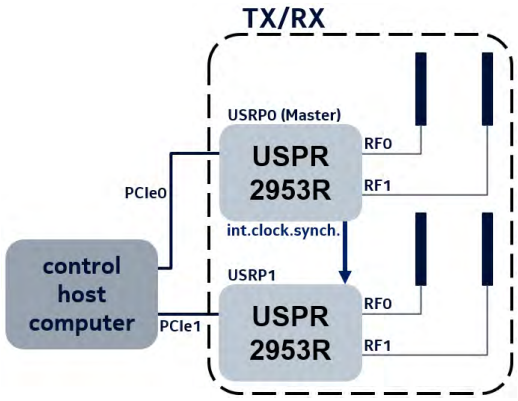

FIGURE 1. Testbed node architecture with 1 control host computer and 2 synchronized SDR transceiver boards (4 fully-synchronous RF ports in total).

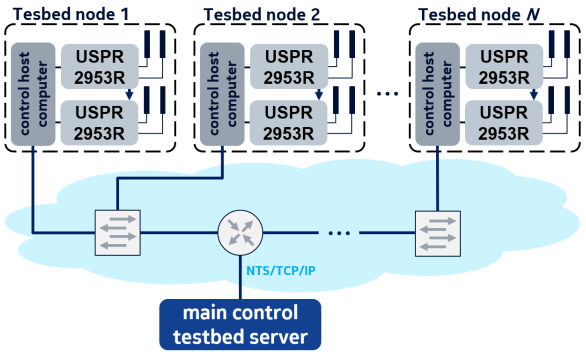

FIGURE 2. Ethernet-based general control system architecture.

II. SYSTEM DESIGN

The conceived distributed sounding system is comprised of multiple cost-effective testbed nodes, each of them built from two SDR boards connected to a host computer through high-speed PCI Express (PCIe) interface, as illustrated in Figure 1. Each board consists of two full-duplex transmitter and receiver channels. Within each node, the board clocks are synchronized in a master/slave configuration by using the 10 MHz clock signal provided by the master, ensuring synchronous transmission or reception, over the 4 radio frequency transceiver antenna ports. Our primary aim is to design a system which can measure the composite channel of multiple links among different nodes deployed at different locations, capturing the overall radio propagation effect of a given environment within the coherence time of the channel. Achieving such a system design has some associated challenges, mainly related to managing the multiple testbed nodes for having a consistent set of channel measurements, and to coping with the limitations of SDR devices to ensure an accurate channel estimation.

One of the primary challenges using multiple testbed nodes is how to automatize the system in order to minimize the effort of controlling the testbed nodes and set the different operational parameters. To that end, we employ the general control system architecture presented in Figure 2, where each of the individual testbed nodes is connected to the main control testbed server by means of a local Ethernet network. The connection is based on TCP/IP sockets to make sure that the testbed server controls multiple testbed nodes with high reliability. In order to measure the composite radio channel, we propose a time division multiplexing (TDM) scheme where one testbed node transmits at a time, in order to discriminate the channel measurements of different links. During the channel measurement operation, the testbed server assigns a single testbed node to transmit the sounding reference signals (e.g., pilot signals which are known to both transmitter and receiver) in a specific time interval, whereas the other nodes are receiving and demodulating the reference signals for estimating the radio channel response. This procedure is repeated in a time-interleaved fashion until each node has transmitted the reference signals, and the channel response between all possible combinations of the testbed nodes is measured.

The testbed nodes are required to be time-synchronized to control the proposed TDM operation, and ensure consistent channel measurements among multiple testbed nodes. This is achieved by pre-synchronizing all testbed nodes at the beginning of each run by employing a proprietary Network Time System (NTS) protocol [22]. NTS is a robust, virtually fail-safe, client/server software, operating as background service and ensuring that the testbed node clock is aligned with the clock of the main control testbed server. By using such protocol, a very tight and stable time-alignment in the order of 1-2 ms is achieved over Ethernet. This constitutes an increased level of accuracy as compared to standard Network Time Protocol (NTP) which typically delivers synchronizations in the order of tens of milliseconds [23].

Once the general multi-node TDM control scheme is in place, the next challenge is the management of the multi-link measurement (e.g., 4×4 channel links) between each pair of testbed nodes. Two different schemes were considered for managing the transmission of the reference signals over the 4 antenna ports at each testbed node: TDM, or frequency-division multiplexing (FDM). In the TDM approach, the reference signal is transmitted in a time-interleaved fashion over multiple antenna ports [24]. By contrast, in the FDM approach, the antenna ports map the reference signal over orthogonal frequency interleaved patterns which span the entire available bandwidth [25]. The FDM approach has an advantage in decreasing the time duration of the reference signal transmission per testbed node, compared to the TDM approach. However, for a fixed bandwidth used for the reference signals transmission, the FDM approach decreases the maximum resolution of the channel response estimation in the frequency domain, which will further decrease the maximum channel delay that can be estimated. Therefore, the design solution presented in this paper, is to use the TDM approach for managing the transmission of the reference signals over the multiple antenna ports.

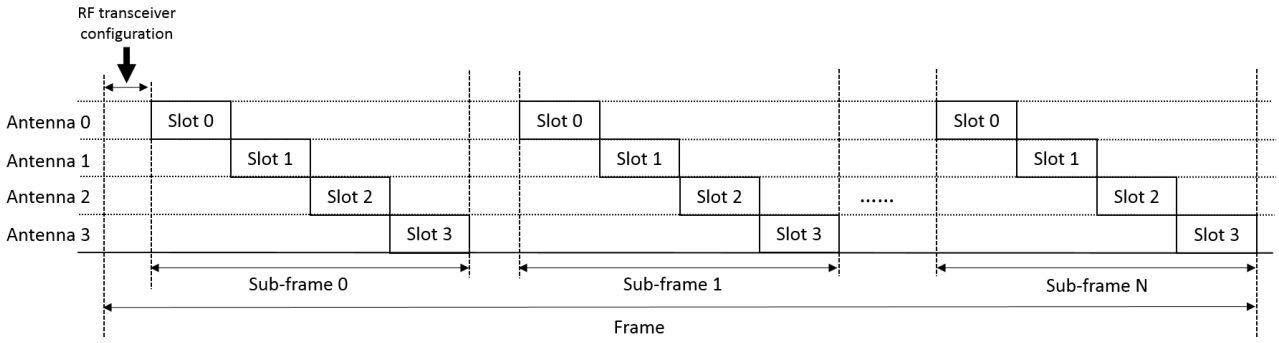

FIGURE 3. TDM frame structure considering *N* subframes (with 4 time slots each) and their corresponding re-synchronization/re-configuration periods.

The overall time frame structure of the channel sounder system, resulting from applying the TDM scheme for multi-node and multi-antenna transmission management, is shown in Figure 3. A frame accounts for the time duration required for the transmission and acquisition of the reference signals between all possible combinations among the testbed nodes, including the time required for configuring the RF transceiver channels of the testbed nodes. A frame consists of N subframes, where N equals to the number of testbed nodes in the system. During one subframe duration, only one testbed node is transmitting the reference signals, while all others are receiving them. At the same time, each subframe is divided into 4 time slots, accommodating the TDM transmission of the reference signals over the four antenna ports of an individual testbed node.

Note that the millisecond accuracy achievable with the aforementioned NTS solution sets restrictions on the time slot duration, which should be sufficiently long to ensure a synchronization time margin for correct measurements. An extended time slot duration translates to an extended frame duration. Since a proper characterization of the composite channel subsumes such channel to remain static within a frame, the applicability of the channel sounder may be restricted to static environments, or to environments whose coherence time is estimated to be significantly larger than the frame duration. These facts will be further discussed in the following section.

The combination of NTS protocol and control over Ethernet to provide the baseline synchronization to the TDM testbed measurement operation scheme was carefully selected. Other control alternatives were explored during the design phase, but their performance was proven to be significantly worse. For example, keeping the local area architecture and using a dedicated WiFi network instead of Ethernet links, the synchronization accuracy dropped to approximately 20 ms on average, even reaching 100 ms in some of the tests. Another alternative would have been to distribute a locally generated high precision clock reference synchronization signal among all the nodes. This solution may reach accuracies at sub-millisecond level and therefore enable the possibility of characterizing composite channels with limited coherence time. However, in a cost-effective distributed measurement system, as the one presented in this paper, its implementation would be rather complex and expensive if built over rubidium clocks or optical cables; or quite limited in measurement distance range if built over RF clock distribution cables [10], [26]. GPS-based synchronization was not an option either. The testbed is designed for reliable indoor use in deployment scenarios associated to some of the new 5G application areas, e.g., in deep indoor clutter conditions within factories, where GPS signals are, in general, not available. By using an Ethernet cabled control network instead, we achieve a good trade-off between synchronization accuracy and measurement distance range, as we are able to span our distributed measurement system over several hundreds of meters by deploying a small switch-based network [27].

We have, until now, discussed the design solutions regarding the challenge of coordinating multiple testbed nodes with the aim of collecting consistent channel measurement samples using SDR devices. However, the SDR devices present some limitations regarding long-term clock stability, phase noise, and receiver dynamic range, which may distort the channel measurements if they are not properly addressed. In order to cope with such limitations, all testbed nodes are re-synchronized during the RF transceiver configuration (cf. Figure 3) before a new node begins its transmission to cope with the long-term clock instability. Further, we propose to transmit a large number of repeated similar reference signals in each time slot, to increase the receiver dynamic range by coherently averaging received reference signals. To cope with the phase noise, we consider sufficient subcarrier spacing in our multi-tone sounding reference signal. All these design aspects will be discussed in detail in the coming section.

We would like to highlight that, by using the proposed distributed architecture and frame design, the testbed could be easily upgraded to include real data transmissions among the nodes by replacing the sounding reference signals with any other customized signal carrying data. Also, the system allows for live demonstration of network algorithms for e.g. interference coordination, which are based on instantaneous mapping of the real-world measurements to relevant

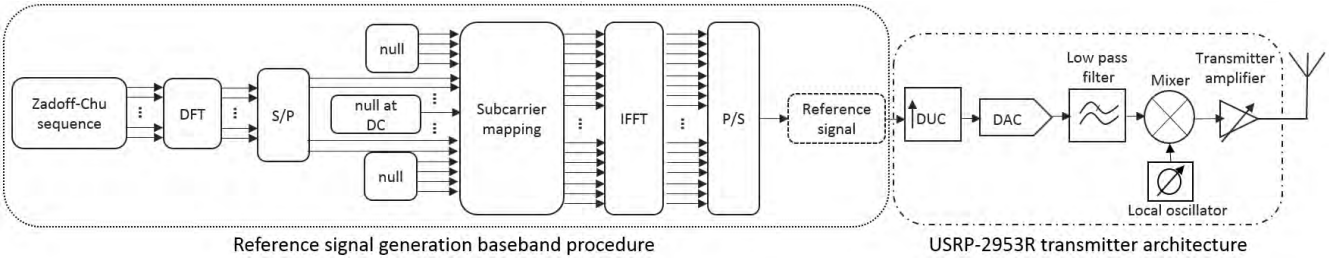

FIGURE 4. Transmitter chain for reference signal generation.

key-performance indicators (KPIs). Similarly, it enables the usage of hybrid simulations, where the obtained measurements can replace standard channel models used for system-level analysis [28], [29]. We see these two aspects as positive design-enabled benefits that also make a difference with respect to the systems reviewed in the previous section.

III. SYSTEM IMPLEMENTATION

In this section, we discuss the applied signal processing procedures at both transmitter and receiver side for accurate estimation of the channel response using the SDR platforms. Besides, the section illustrates the implementation-specific aspects, including the system parameter numerology selected as a reference for our multi-node multi-antenna sounding setup.

A. REFERENCE SIGNAL GENERATION

The reference signals used for channel estimation are built by mapping Zadoff-Chu (ZC) sequences [30] over Orthogonal Frequency Division Multiplexing (OFDM) symbols. ZC sequences are selected thanks to their property of having constant amplitude over the dual time/frequency domain. A constant time domain amplitude allows using a limited power back-off at the transmitter for counteracting signal distortions due to e.g. digital clipping and non-linear power amplifier response, translating to a higher transmit power. A flat frequency domain response translates to zero autocorrelation, which improves channel estimation and time synchronization. ZC sequences are also used by many radio standards, including the uplink of 3GPP long-term evolution (LTE) [31].

The block diagram of the reference signal transmission is shown in Figure 4. A ZC sequence is converted to frequency domain via Discrete Fourier Transform (DFT), and the resultant vector is mapped over the set of subcarriers which represents the transmission bandwidth. Zeros are padded at the edges of the bandwidth to limit the out-of-band spectral interference. Also, the direct current (DC) subcarrier is nulled for circumventing the DC signal leakage. The baseband time domain signal is finally generated via Inverse Fast Fourier Transform (IFFT). Such transmitter architecture allows preserving the flat frequency response of the original ZC sequence in the bandwidth of interest. The time domain amplitude of the signal may still have minor fluctuations, which appear due to the mismatch between ZC sequence length and IFFT size. This will be further discussed in the next section.

The generated baseband reference signal is then streamed to the RF board via the PCIe connector. The board up-samples the digital signal and converts it to an analog RF signal for transmission over the antenna. Four antennas are employed in each testbed node, and the transmission of the reference signals over each antenna is performed in a time-interleaved fashion as discussed in the above. In order to discriminate the different antenna links for channel estimation, two reference sequences are employed, where one of the sequences is mapped to the first antenna port (first time slot in the subframe), and the other sequence is mapped to the other three antenna ports (second, third and fourth time slots). Then, at the receiver side, the signal transmitted over the first antenna port is identified via cross-correlation using the first reference sequence, whereas the other slots are identified based on the predefined TDM subframe structure. The use of a difference sequence for the first, resolves any ambiguities with respect to the antenna sequence used for transmission.

One reference signal is transmitted over an OFDM symbol, and repeated a large number of times to fit a predefined time slot duration. Such redundancy offers a margin for the time synchronization between transmitter and receiver nodes. Transmitting repeated identical symbols per time slot allows the receiver processing to benefit from signal cyclicity. As explained later, this also provides a prominent advantage for estimating the frequency offset at the receiver side, by observing the phase shift of consecutive repeated OFDM symbols. Also, we can benefit from the transmission of consecutive repeated OFDM symbols to increase the receiver dynamic range of the SDR platform, by exploiting coherent averaging [32] over an assumed static channel.

B. RECEIVER PROCESSING

The aforementioned lack of a tight synchronization may rise challenges concerning frequency instability and residual time misalignment between the transmitter and receiver boards. To address these challenges, and ensure accurate channel estimation using SDR devices, the receiver digital signal processing shown in Figure 5 is employed.

At the receiver end, the node receives the RF signal on each antenna ports and down-converts it to a complex digital

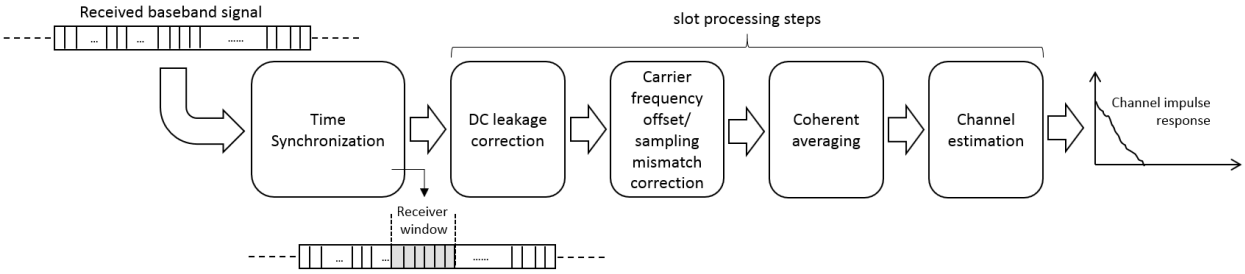

FIGURE 5. Baseband processing operations at receiver side.

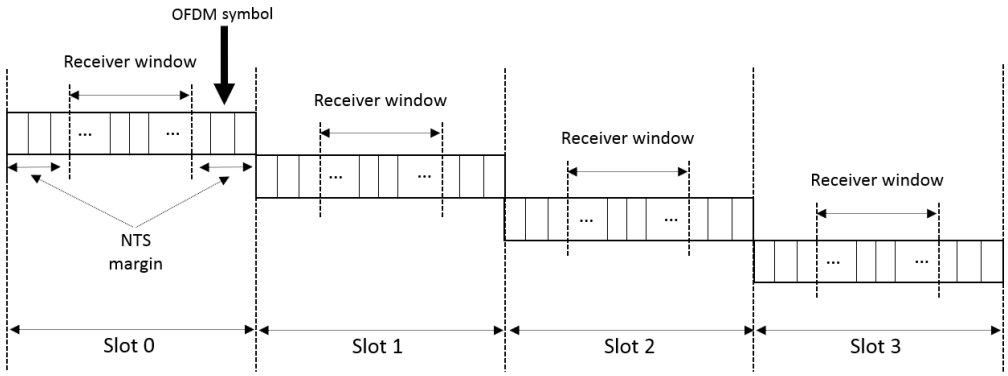

FIGURE 6. Subframe structure with possible receiver window position.

baseband signal (I/Q signals) using the SDR RF boards. The I/Q signals are streamed to the host PC, where the digital baseband signal processing is carried out. First, the time synchronization is performed using cross-correlation between the received signal and a copy of the transmitted reference signal, to find the position of the first useful sample of the received signal. Then, DC leakage cancellation, correction of the carrier frequency offset and sampling clock mismatch are performed in each time slot. Afterward, a coherent averaging can eventually be carried out to increase the receiver dynamic range, before channel estimation is performed. Such steps are described in more detail below.

1) TIME SYNCHRONIZATION

The NTS protocol enables a first synchronization among the nodes with accuracy in the order of a millisecond, as described in the previous section. While this may suffice for aligning the nodes at level of a slot interval, further refinements are needed to identify the antenna port mapped over that slot, and to enable a proper time alignment at OFDM symbol level for correct channel estimation. Cross-correlation between the received sequence and the transmitted one is therefore performed. A first cross-correlation operation is applied for identifying the first slot in a subframe. This computation is carried out using the first reference sequence, which was mapped to the first antenna port/time slot. As a result, the first antenna port is identified and OFDM-level symbol alignment for channel estimation is also achieved. To accommodate an error margin of the NTS time synchronization, the receiver window spans only a subset of the repeated OFDM symbols within the time slot, as shown in Figure 6. The receiver window for the following slots is identified by using the known TDM time frame structure, given the periodicity of the system. The size of the receiver window is dimensioned according to the time slot duration, the symbol duration, and the error margin of the NTS time synchronization protocol.

2) DC LEAKAGE

To reduce device cost and the power consumption, SDR receivers are commonly based on a direct-conversion, or zero intermediate frequency, architecture, where the received radio frequency signal is converted directly to baseband. Such receiver suffers from the ''direct current'', caused by the local oscillator leakage. To reduce its impact, we implemented a basic DC leakage cancellation using a notch filter in the frequency domain. Note that the DC subcarrier was blanked at the transmitter.

3) CARRIER FREQUENCY OFFSET

Since transmitter and receiver are not sharing the same oscillator, carrier frequency offset may affect the performance of the sounding system. To deal with the carrier frequency offset, we employ the maximum likelihood estimation (MLE) scheme proposed in [33]. The scheme estimates the frequency offset by observing the phase shift of the subcarriers between

consecutive repeated OFDM symbols, and use the estimated values to counter-rotate the subcarrier phase accordingly.

4) SAMPLING CLOCK MISMATCH DRIFT

Besides the carrier frequency offset, the lack of a common reference clock at the transmitter and receiver induces a sampling frequency mismatch. That leads to a drift in the time synchronization between the consecutively transmitted OFDM symbols. To overcome this, a cross-correlation in the time domain is applied to estimate the timing offset of each received symbol, in relation to an arbitrarily chosen received reference symbol. Assuming that the drift within a symbol is small, the offset/drift is corrected on a per symbol basis, by correspondingly counter-rotating the subcarrier phases in the frequency domain [34].

5) COHERENT AVERAGING

Typically, the SDR device receiver dynamic range is limited (i.e., the employed SDR platform receiver dynamic range is ideally 86 dB, considering a 14 bit resolution of the ADC [21]). This may represent a limitation for the sounding system capability in measuring large path losses. To increase the receiver dynamic range, we employ coherent averaging of several consecutive received symbols, assuming that frequency offset and sampling clock mismatch have been properly corrected, and the channel is static during the receiver window. This allows reducing the noise power while maintaining constant the useful signal power. For instance, with 1000 consecutive symbols being averaged, the sounding system dynamic range can be increased up to 30 dB, due to the resulting processing gain of the coherent averaging [32]. Note that such gain in terms of dynamic range cannot be achieved in case the scenario is dynamic within the receiver window. The stationarity properties of the channel therefore affect the size of the receiver window used for coherent averaging.

6) CHANNEL ESTIMATION

The channel frequency response is estimated using a least square estimator, over the subcarrier positions, where the ZC sequence is mapped. The frequency response of the DC subcarrier is computed by interpolating the response of the neighboring subcarriers. The channel impulse response can in principle be computed using an IDFT operation, on the estimated channel frequency response. However, this operation leads to low resolution and side lobe leakage effects, that are exacerbated by the relatively low bandwidth of the testbed. To overcome these limitations, we apply parametric channel modeling [35], which works by fitting a sum-of-spikes representation of the channel impulse response to the observed signal. The superfast line spectral estimation (SF-LSE) algorithm [36] is used for estimating the parameters (model order, delays, and coefficients) of the parametric channel model. This type of method is known as a super-resolution approach, because it allows the multipath components to be estimated with a higher delay resolution, than the reciprocal of the bandwidth, as is approximately the case when using the IDFT. The parametric approach also avoids the presence of sidelobes as in the case of IDFT operation.

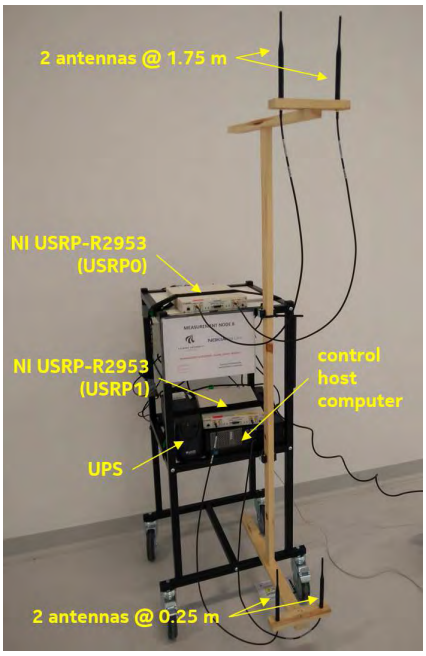

FIGURE 7. Testbed node physical setup. Trolley-based implementation considering a distributed antenna configuration with 2 antennas at two different heights (0.25 and 1.75 m).

C. SYSTEM CONFIGURATION AND SYSTEM PARAMETERS

The main parameters of the sounding system are summarized in Table 2, where we highlight both the general configuration parameters and the reference numerology which has been used in the activities described in Sections IV and V.

The implemented sounding system consists of 12 SDR testbed nodes, each of them with the physical configuration displayed in Figure 7. The specific trolley-based implementation, complemented by an uninterruptible power supply (UPS), facilitates a quick and easy redeployment of the nodes during the measurement. The antenna configuration per testbed node of 2 antennas at two different heights (0.25 and 1.75 m) is chosen with the target of using the system for characterizing the channel at different spatial positions at given physical locations. Carrier frequency-wise, the main goal of our activities was the evaluation of radio propagation at two ISM bands (e.g, 2.45 and 5.8 GHz). Therefore, for this reference implementation of the testbed, the carrier frequencies configured were 2.3 and 5.7 GHz, as they were the closest frequency allocations possible ensuring interference avoidance with/from other coexisting radio systems. Moreover, the spacing between antennas is dimensioned to be larger than half of a wavelength at the lower frequency (6.52 cm), aiming to de-correlate the set of measurement samples from each antenna at both frequencies of operation.

As per the general system design considerations given in Section II, the number of subframes in the TDM frame structure (cf. Figure 3) is set equal to the number of testbed nodes available for measurement. Every testbed node is assigned a single transmission subframe, which allows for the broadcast of the reference signals over its 4 antenna ports in 4 consecutive time slots. Simultaneously, the other 11 subframes are used for reception. Before the testbed nodes are allocated a subframe for transmission or reception, the configuration of the RF transceivers channel is carried out, and also re-synchronization of the testbed nodes clock to keep the clock timing stability of the system. These operations are performed within a 10 ms interval. Considering a predefined time slot duration of 25.6 ms, the subframe duration is set to be 4×25.6 ms $=$ 102.4 ms. Overall, the transmission and reception of the reference signals among all 12 testbed nodes are performed over one full frame duration of approximately 1.35 s. Such frame execution will be carried out per single deployment of the tested nodes, enabling the collection of $12\times11\times4\times4 = 2112$ independent link samples. Thus, considering a number of re-deployments, a large number of spatially distributed channel measurement links can be effectively collected within a short period of time.

The specific sounding implementation employs ZC reference sequences mapped over OFDM symbols. In this case, the reference sequence length is chosen to be 601 samples, which are mapped over the center of the bandwidth. We consider a FFT size of 1024 and we set a 40 MHz sampling rate, leading to a 39.06 kHz subcarrier spacing. The resulting baseband signal was shown to have minor envelope fluctuations, not larger than 2 dB. The signal presents an overall bandwidth of 24 MHz, which translates into a time resolution of 1/24 MHz = 41.66 ns. However, in practice, this resolution can be improved by means of SF-LSE, as detailed in Subsection III-B.6. The subcarrier spacing is sufficiently large for coping with the phase noise of the employed SDR devices. Given the 1/39.06 kHz $\approx$ 25.6 μs symbol duration, 1000 symbols can be mapped over the 25.6 ms slot. This large number of symbols allows us to increase the dynamic range of the receiver by 29.5 dB, considering 900 effective symbols per receiver window (cf. Figure 6) are used for coherent averaging, and the remaining received symbols are used as error margin (1.25 ms) for counteracting the possible NTS time synchronization misalignment. By configuring the reference level of the receiver window (which fixes the RX gain to a proportional value to the specific expected signal input level) to its minimum value of -25 dBm, and applying coherent averaging, we are able to increase the sensitivity of the measurement system from -111 dBm to -140.5 dBm. The output TX power is set to $+6.4$ dBm at 2.3 GHz and $+5.2$ dBm at 5.7 GHz. It was verified that these levels avoid the appearance of non-linear distortion effects, thanks to the limited envelope fluctuations of the signal.

To ensure the consistency of different measurement samples across multiple SDR devices, a thorough calibration of the devices is performed during the implementation of the system. Figure 8 shows the result from a back-to-back test with two RF ports from two different boards. Due to hardware imperfections, the normalized amplitude response exhibits a slight attenuation over the considered measurement bandwidth (24 MHz). Such behavior is observed for the different boards at both considered carrier frequencies, with an average maximum variation of 0.5 dB among all carried tests. To ensure that such variation does not affect the quality of the channel estimation, we performed an extensive individual calibration measurement among all RF ports from all sounder devices, at both frequencies of interest - in both TX and RX mode, and then used the results to compensate for the device-specific variations during the receiver data processing procedures. The results from the calibration test across all SDR devices indicated a similar average TX power and RX gain performance at both frequencies of operation, with a standard deviation of 1.3 and 1.6 dB, respectively.

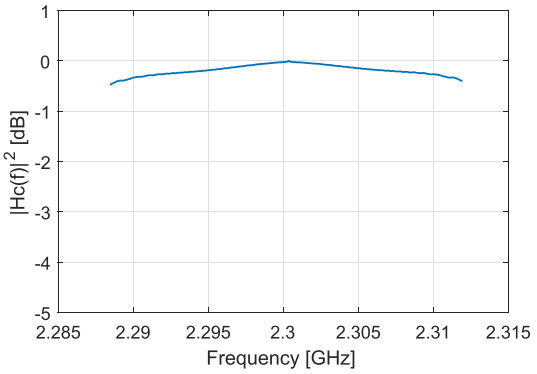

FIGURE 8. Normalized frequency amplitude response of two interconnected RF ports from two different USRP boards at 2.3 GHz.

All other physical elements considered in the implemented setup were also calibrated (cf. Figure 7). The Wanshih Electronic WSS007 dual-band dipole antennas, with 2 dBi peak gain at both frequency bands according to specifications [37], exhibited a quasi-isotropic mean effective gain of approximately 1.28 dBi at 2.3 GHz and 0.39 dBi at 5.7 GHz in an anechoic chamber calibration measurement. The attenuation introduced by the coaxial cables interconnecting the different RF ports to the antennas was also measured, finding values of 2.4 and 3.3 dB at 2.3 and 5.7 GHz, respectively. Altogether, the reference configuration of the testbed implemented allows for maximum link loss measurements of 134.7 dB at 2.3 GHz and 129.9 dB at 5.7 GHz, ensuring sufficient measurement dynamic range to cover TX-RX distances in the range of a few hundred meters, even in dense clutter conditions.

IV. SYSTEM VERIFICATION

To validate the proposed SDR USRP-based channel sounding procedures and demonstrate the measurement capabilities of the system, we performed different verification tests. These tests had two different aims: 1) to verify the accuracy of the system in terms of channel impulse response estimation; and 2) to verify the accuracy of the system in terms of

TABLE 2. Reference configuration of the multi-node multi-antenna channel sounder.

Parameter	General Design	Reference Configuration
Number of testbed nodes	N	12
Antenna configuration per node	4x4 MIMO, fully flexible	2x2 MIMO @ 2 antenna heights
Carrier frequencies	1.2-6 GHz	2.3 GHz / 5.7 GHz
Sounding signal	multi-tone	OFDM
Reference sequence	flexible	Zadoff-Chu (ZC)
Sampling rate	flexible, max. 40 MS/s	40 MS/s
Subcarrier spacing	flexible	39.06 kHz
Length of the reference sequence	flexible	601
FFT size	depends on sampling rate and reference sequence size	1024
Symbol duration	depends on subcarrier spacing	25.6 μs
Signal bandwidth	depends on reference sequence length and subcarrier spacing, max. 40 MHz	24 MHz
Temporal resolution	depends on signal bandwidth	41.66 ns (* improved by SF-LSE)
Slot duration	depends on symbol duration and number of symbols transmitted	25.6 ms (1000 symbols)
Receiver dynamic range	86 dB (14 bit resolution)	115.5 dB (900 symbols)
Receiver window reference level	flexible, max. 0 dBm, min. -25 dBm	-25 dBm
Transmit power per branch	flexible, depends on carrier frequency, max. +10 dBm	+6.4 dBm @ 2.3 GHz +5.2 dBm @ 5.7 GHz
Antenna type	flexible	Vertical dipoles, 2 dBi peak gain 1.28 dBi effective gain @ 2.3 GHz 0.39 dBi effective gain @ 5.7 GHz
Cable type	flexible	1 m long RF flex coaxial cables 2.4 dB @ 2.3 GHz 3.3 dB @ 5.7 GHz
Maximum measurable path loss	depends on transmit power, receiver window reference level, receiver dynamic range, antenna type and cable type	134.7 dB @ 2.3 GHz 129.9 dB @ 5.7 GHz

measured received power to perform path loss estimation. All tests were done with the reference configuration detailed in Section III and summarized in Table 2.

A. CHANNEL IMPULSE RESPONSE

The objective of the first test is to verify the sounder system capability of estimating resolvable temporal multipath components (taps) accurately. This test has also the aim of confirming the potential of the employed channel estimation approach (i.e., superfast line spectral estimation, SF-LSE), in comparison with the commonly used IDFT-based estimation. The test measurement was conducted by using a standard multi-tap channel emulator, connected between two RF ports of two different boards belonging to different testbed nodes, one acting as the TX and the other as RX.

We tested two cases. First, the channel emulator was configured to emulate two multipath components with equal power and separated by 22 ns. In the other case, the second multipath component was configured to be 10 dB lower than the first component. Figure 9 displays the results from the two tests. Both plots illustrate the configured multipath components (blue diamonds), and the estimated components using the standard IDFT operation (magenta lines) and the SF-LSE approach implemented in our system (red stars). In both cases, by using the superfast parametric approach, we can resolve correctly the two multipath components in both delay (with ± 5 ns deviation) and amplitude (with a maximum deviation of 0.97 dB). This result demonstrates the capability of the SF-LSE in resolving taps that are separated by delays below the temporal resolution set by the signal bandwidth (41.66 ns), thus achieving an effective increase of the temporal resolution.

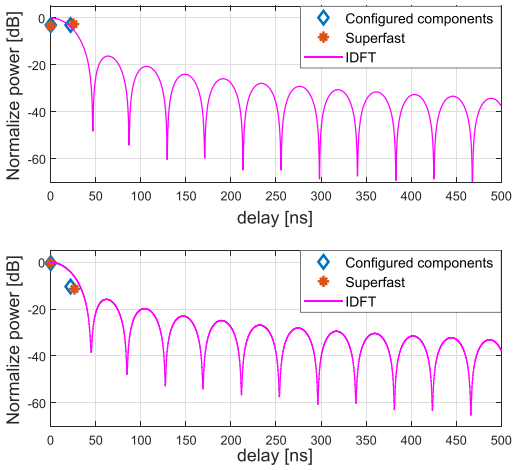

FIGURE 9. Results of the channel impulse response verification test with channel emulator configured with two taps with equal amplitude (above), and 10 dB difference in amplitude (below).

For further verification, we also tested the case where the channel emulator is configured with a reference standard channel model. We selected the ITU-R indoor office channel model (Channel A) [38], with a fixed power delay profile and larger excess delay compared to the previous cases. The 6-tap configuration of the model is as follows: relative delay of 0, 50, 110, 170, 290 and 310 ns, and average power of 0, -3, -10, 18, -26 and -32 dB. The results from this test are presented in Figure 10. Similarly to the previous case, the figure depicts the original channel model taps and the estimated taps using both the SF-LSE approach and the IDFT operation. In this case, once again, the IDFT operation is not able to resolve the taps, due to the side lobe leakage.

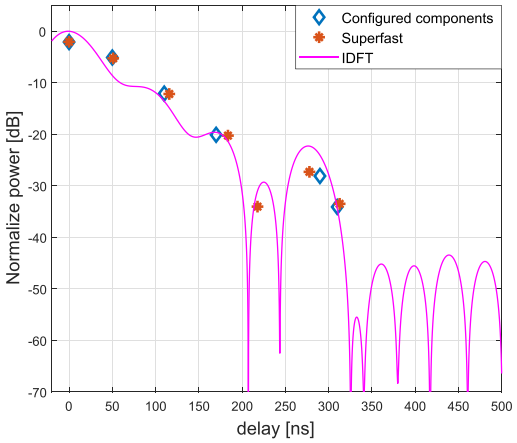

FIGURE 10. Results of the channel impulse response verification test with channel emulator configured with the 6-tap ITU-R indoor office channel model (Channel A).

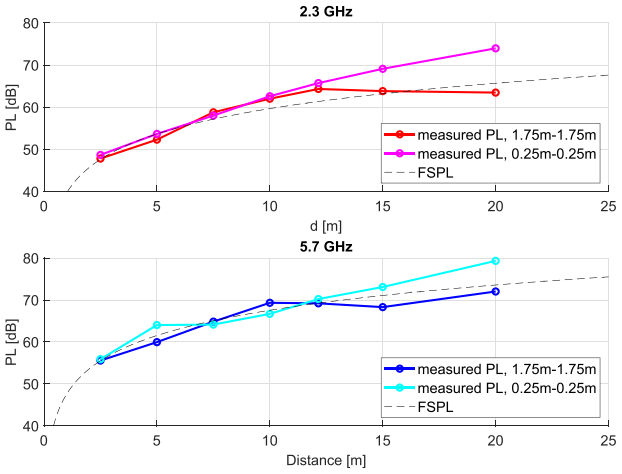

FIGURE 11. Results of the path loss verification test in line-of-sight free space conditions for two antenna height configurations (higher link at 1.75 m, and lower link at 0.25 m) at both configured testbed carrier frequencies (2.3 and 5.7 GHz).

On the contrary, the superfast parametric channel modeling approach can resolve the configured taps with a standard deviation of 5.7 ns in delay and 0.5 dB in amplitude. Still, one can notice the presence of an extra component at around 220 ns delay, that also corresponds to a sidelobe of the IDFT estimation. This is a processing artifact limitation of the SF-LSE algorithm in estimating low energy components with high accuracy. However, given the low energy of the artificial component, the impact of such inaccuracies on the channel estimation quality is minimal. This ratifies the capability of the sounder of accurately estimating the channel impulse response, and supporting even super-resolution techniques.

B. RECEIVED POWER AND PATH LOSS

The second test aims at verifying the accuracy of the sounding system in performing power measurements and path loss estimation. In order to test that, we performed a line-of-sight (LOS) over-the-air measurement in a large open space where free space conditions apply. The measurement was performed by deploying one of the testbed nodes at a fixed location, and second one at a variant distance (2.5, 5, 7.5, 10.0, 12.5, 15 and 20 m).

Figure 11 shows the power measurement test results in terms of path loss (PL) as a function of the distance between nodes for both configured carrier frequencies (2.3 and 5.7 GHz), considering the two different antenna heights configurations (0.25 and 1.75 m) applied at both transmitter and receiver nodes. Each of the PL values was estimated by integrating the received power over the operational bandwidth, and averaging the results from all the individual 8 links at a given position (e.g., to average fast-fading effects by taking into account all possible links between the two nodes at each particular height). Each of the individual link measurements is independently calibrated in the receiver data processing stage, accounting for any device-specific deviations, as it was explained previously in Section III-C (i.e., subtracting the average measured RX power from the calibrated RF port-specific TX power, and compensating by the also calibrated RF port-specific RX gain imperfections, effective antenna gains and cable losses at the particular frequency of operation). The results indicate that the measured PL follows the free space path loss (FSPL) reference [39], with standard deviations of 0.79 and 0.82 dB for 2.3 and 5.7 GHz, respectively, for the case where the antennas are mounted at a 1.75 m height. In the case of the lower antenna configuration (antennas mounted at 0.25 m), a similar behavior is observed for the short distances, while for distances larger than the theoretical breakpoints (6 m at 2.3 GHz, and 15 m for 5.7 GHz), an increase in PL is observed due to the effect of the ground reflection.

Overall, these test results are very well aligned with the expected behavior as a function of distance range, carrier frequency, and antenna height. This endorses the measurement capabilities of our sounder in performing accurate power estimation and therefore an accurate path loss characterization.

V. EXPERIMENTAL RESULTS

Until now, we have detailed the different design, implementation and verification aspects of our multi-node multi-antenna channel sounder. In this section, we demonstrate the agility of our system for effectively collecting large data sets of measurement data without the need for an excessive number of laborsome redeployments. By using our proposed measurement system in a given scenario, we can simultaneously collect samples at multiple distributed spatial locations, allowing for an accurate statistical characterization of the composite radio channel.

In order to illustrate the above-mentioned, we present the results from a field test performed in an industrial setting. The selected scenario (Smart Production Lab, at the Department of Mechanical and Manufacturing Engineering, Aalborg University) is closely related to those considered in the 5G new application areas described in the

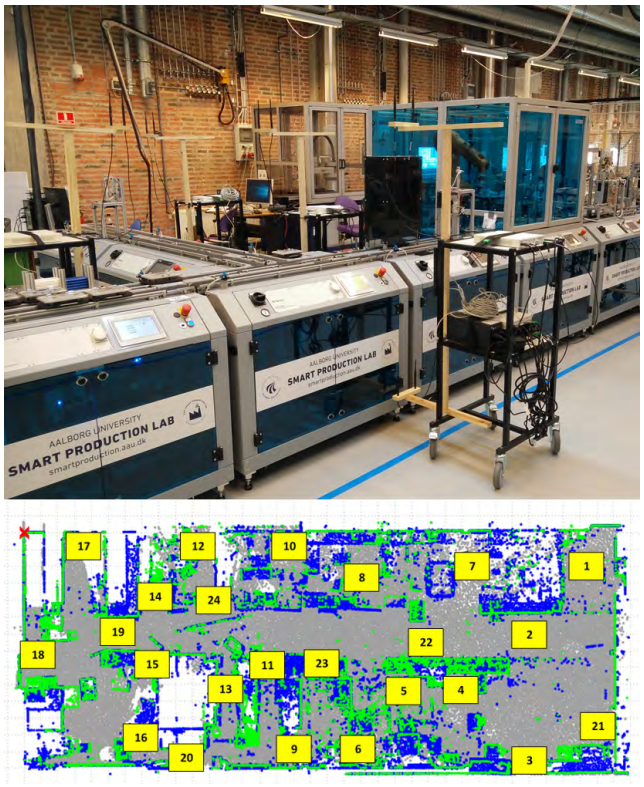

FIGURE 12. Overview of the industrial measurement scenario: testbed nodes deployed at some of the measurement positions (above), and measurement positions indicated over a plane-cut of a 3D laser scan of the industrial facility (below).

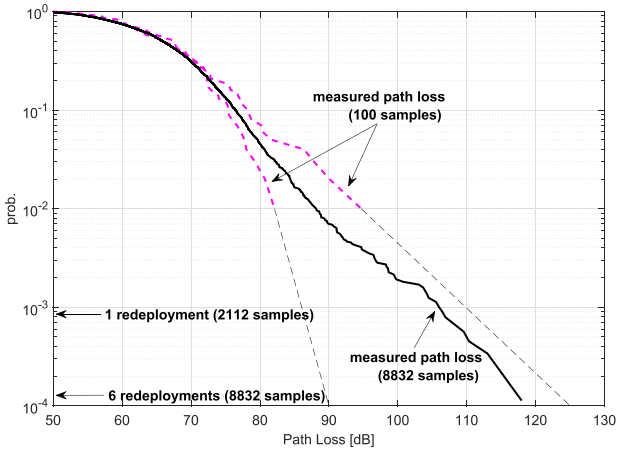

FIGURE 13. Empirical complementary cumulative distribution functions of measured path loss in an industrial production lab facility at 2.3 GHz.

introduction (i.e. factory automation). The measurements were performed at 24 selected locations which were approximately uniformly spatial-distributed across the facility, based on a visual inspection and considering potential deployment positions of controllers, sensors, and actuators in such industrial automation scenario. The size of the facility is $20\times40\times6$ m. Such dimensions imply a maximum possible measurement distance of approximately 45 m, which is well within the measurement distance range capabilities of the system. To illustrate the type of factory clutter explored in the measurements, a picture of the scenario and the associated floor plan with the measurement locations are displayed in Figure 12. Further details about the scenario and the measurement campaign can be found in [40].

To measure all the $24\times23 = 552$ possible links between these 24 spatial positions using a standard approach (e.g., with a single fixed transmitter and a mobile receiver) requires a large number of redeployments (i.e., more than 200) which translates also into a big effort in terms of overall measurement collection time. By using our multi-node multi-antenna system, with 12 nodes, we were able to reduce the effort to only 6 redeployments, with an approximated total measurement time of approximately 3 h (considering the time spent in the initial deployment, measurement collection at the two considered carrier frequencies and the different redeployments). The initial deployment of the 12 nodes and the Ethernet control network takes approximately 1 h. After the first measurement snapshot, each of the 5 remaining redeployments was carefully planned to minimize the number of changes in node positions needed to sweep all the possible spatial combinations. In each redeployment, a maximum number of 8 nodes (and their associated Ethernet control cables) was moved, resulting in an average redeployment time of approximately 20 min. It should be highlighted that such fast re-deployment time is partly achieved by the use of the UPS units in each of the nodes; as they allow a smooth transition between measurement points without the need of powering the nodes off and thus, without the need of manually re-booting and re-configuring the USRP boards.

Considering the 24 measurement locations and the 4 different spatial positions of the antennas at each node, we collected a total number of $24\times23\times4\times4 = 8832$ samples. With such large number of independent samples, obtained in a spatially-distributed manner, it is possible to get a deep insight into the overall radio propagation behavior across the industrial scenario, statistically characterizing the channel at levels close to the 10^{-4} percentile. Those levels (and lower) are typically the percentiles at which the effects of rare events are captured in the tails of the channel distributions, and thus it is of great importance to have enough relevant empirical data to characterize them. If radio network planning is done based on channel distributions derived from empirical sets with limited number of samples, there is a risk of being inaccurate, experiencing significant deviations in the radio signal availability and reliability predicted for a given scenario.

In order to illustrate this fact, we display three different empirical channel distributions in terms of 2.3 GHz measured path loss in Figure 13. The two first distributions (thick dashed magenta lines) are obtained by randomly and independently selecting a low number of samples from our measurement (i.e. 100 samples), while the remaining (thick solid black line) considers the full data set of 8832 sam-

ples. We have selected such cases for brevity, to illustrate the extreme cases of the above-discussed. In this case, the distributions based on the low number of samples, result in a ±6 dB deviation from the distribution extracted from the large measurement data set at the 10^{-2} percentile, representative of the 99% of signal availability. Moreover, by extending the tails of the distributions (thin dashed black lines) based on the low number of samples, as is typically done to get an indication of the behavior at lower percentiles [41], it is possible to observe the considerable deviation from the more reliable distribution computed over all samples. In the path loss pessimistic case, at the 10^{-4} percentile (99.99% signal availability), the deviation is still bounded by the +6 dB deviation. However, in the optimistic case, this deviation can be as much as 30 dB from the ''sample truth''. Clearly, if radio network planning for the wireless factory (which should be robust and reliable), relied on models, or empirical evidence deviating this much, the integrity of the factory automation would be at risk.

The described activity confirms the unique capability of our multi-node multi-antenna channel sounder in characterizing radio propagation in potentially large and complex scenarios with limited human effort. This paves the way for an agile characterization of relevant scenarios for future 5G systems.

VI. CONCLUSIONS AND FUTURE WORK

We have presented a distributed multi-node multi-antenna channel sounder based on universal software radio peripheral (USRP) boards. Our flexible design is meant to measure all channel links among all the nodes in the system, generating large sets of measurement samples useful for characterization of radio propagation in a given environment with limited human effort. In particular, the current setup of the sounder consists of 12 nodes with up to 4×4 multiple input multiple output (MIMO) antenna capabilities, and is able to measure up to 2112 independent radio links per deployment in ∼1.35 seconds. The major challenges for the design of the channel sounder are related to testbed management, synchronization of the nodes, overcoming non-idealities of the SDR hardware and signal processing design for accurate channel estimation. These have been thoroughly discussed in the paper, along with our proposed solutions. System verification and preliminary experimental results have also been presented.

Our future research activities target the usage of the multi-node multi-antenna channel sounder for an extensive evaluation of radio propagation in diverse scenarios in light of the novel 5G use cases. Also, the possibility of further improving the system performance will be pursued. In particular, synchronization solutions such as Precision Time Protocol (PTP) are to be explored, given their promise of significantly reducing the residual timing errors, translating to significantly shorter frame duration and therefore the possibility of tracking time-varying channels.

ACKNOWLEDGMENTS

The authors would like to thank Emil Jatib Khatib, Postdoctoral Researcher at Aalborg University, Denmark (now with University of Malaga, Spain), for his contribution to the testbed activities and, especially, for conducting the synchronization accuracy studies.

REFERENCES

[1] *Service Requirements for the 5G System, Stage 1 (Release 16)*, document 3GPP TS 22.261, v.16.5.0, Sep. 2018.
[2] *Study on Channel Model for Frequencies From 0.5 to 100 GHz (Release 14)*, 3GPP TR 38.901, v.14.3.0, Dec. 2017.
[3] B. Chen, J. Wan, L. Shu, P. Li, M. Mukherjee, and B. Yin, ''Smart factory of industry 4.0: Key technologies, application case, and challenges,'' *IEEE Access*, vol. 6, pp. 6505–6519, 2017.
[4] B. Holfeld *et al.*, ''Wireless communication for factory automation: An opportunity for LTE and 5G systems,'' *IEEE Commun. Mag.*, vol. 54, no. 6, pp. 36–43, Jun. 2016.
[5] J. D. Parsons, D. A. Demery, and A. M. D. Turkmani, ''Sounding techniques for wideband mobile radio channels: A review,'' *IEE Proc. I-Commun., Speech Vis.*, vol. 138, no. 5, pp. 437–446, Oct. 1991.
[6] C. L. Holloway, W. F. Young, G. H. Koepke, C. A. Remley, D. G. Camell, and Y. Becquet, ''Attenuation of radio wave signals coupled into twelve large building structures,'' Nat. Inst. Standards Technol., Gaithersburg, MD, USA, Tech. Note 1545, Aug. 2008.
[7] J. Austin, W. P. A. Ditmar, W. K. Lam, E. Vilar, and K. W. Wan, ''A spread spectrum communications channel sounder,'' *IEEE Trans. Commun.*, vol. 45, no. 7, pp. 840–847, Jul. 1997.
[8] MEDAV. *Rusk Channel Sounder*. Accessed: Oct. 2018. [Online]. Available: http://www.channelsounder.de/medavdocs/RUSK-MIMO-Produktinfo-E_W701WI.096_.pdf
[9] P. Pajusco, N. Malhouroux-Gaffet, and G. E. Zein, ''Comprehensive characterization of the double directional UWB residential indoor channel,'' *IEEE Trans. Antennas Propag.*, vol. 63, no. 3, pp. 1129–1139, Mar. 2015.
[10] G. R. MacCartney, Jr., and T. S. Rappaport, ''A flexible millimeter-wave channel sounder with absolute timing,'' *IEEE J. Sel. Areas Commun.*, vol. 35, no. 6, pp. 1402–1417, Jun. 2017.
[11] M. Gahadza, M. Kim, and J. Takada, ''Implementation of a channel sounder using GNU radio opensource SDR platform,'' *IEICE Tech.*, vol. 108, no. 446, pp. 33–37, Mar. 2009.
[12] D. Maas, M. H. Firooz, J. Zhang, N. Patwari, and S. K. Kasera, ''Channel sounding for the masses: Low complexity GNU 802.11b channel impulse response estimation,'' *IEEE Trans. Wireless Commun.*, vol. 11, no. 1, pp. 1–8, Jan. 2012.
[13] A. Merwaday, N. Rupasinghe, I. Güvenç, W. Saad, and M. Yuksel, ''USRP-based indoor channel sounding for D2D and multi-hop communications,'' in *Proc. Annu. IEEE Wireless Microw. Technol. Conf. (WAMICON)*, Jul. 2014, pp. 1–6.
[14] M. N. Islam, B.-J. J. Kim, P. Henry, and E. Rozner, ''A wireless channel sounding system for rapid propagation measurements,'' in *Proc. IEEE Int. Conf. Commun. (ICC)*, Jun. 2013, pp. 5720–5725.
[15] R. Wang, C. U. Bas, O. Renaudin, S. Sangodoyin, U. T. Virk, and A. F. Molisch, ''A real-time MIMO channel sounder for vehicle-to-vehicle propagation channel at 5.9 GHz,'' in *Proc. IEEE Int. Conf. Commun. (ICC)*, May 2017, pp. 1–6.
[16] H. W. H. Jones, P. A. Dmochowski, and P. Teal, ''Channel sounding with software defined radio,'' in *Proc. 16th Electron. New Zealand Conf. (ENZCon)*, Nov. 2009, pp. 1–6.
[17] H. Boeglen, A. Traore, M. M. Peinado, R. Lefort, and R. Vauzelle, ''An SDR based channel sounding technique for embedded systems,'' in *Proc. 11th Eur. Conf. Antennas Propag. (EUCAP)*, May 2017, pp. 3286–3290.
[18] N. H. Fliedner, D. Block, and U. Meier, ''A software-defined channel sounder for industrial environments with fast time variance,'' in *Proc. 11th Int. Symp. Wireless Commun. Syst. (ISWCS)*, Aug. 2018, pp. 1–6.
[19] Ettus Research. *Universal Software Radio Peripheral*. Accessed: Oct. 2018. [Online]. Available: https://www.ettus.com/product
[20] National Instruments. *LabVIEW Communications System Design Suite*. Accessed: Oct. 2018. [Online]. Available: http://www.ni.com/en-us/shop/select/labview-communications-system-design-suite

[21] National Instruments. *USRP-R2953 Software Defined Radio Reconfigurable Device*. Accessed: Oct. 2018. [Online]. Available: http://www.ni.com/en-us/support/model.usrp-2953.html
[22] Softros Systems. *Network Time System*. Accessed: Oct. 2018. [Online]. Available: https://nts.softros.com/
[23] D. Mills, *Network Time Protocol Version 4: Protocol and Algorithms Specification*, document RCF-5905, IETF, Jun. 2010.
[24] D. R. Smith, *Digital Transmission Systems*. New York, NY, USA: Springer, 2004.
[25] S. Weinstein and P. Ebert, "Data transmission by frequency-division multiplexing using the discrete Fourier transform," *IEEE Trans. Commun. Technol.*, vol. 19, no. 5, pp. 628–634, Oct. 1971.
[26] L. Talbi and J. LeBel, "Broadband 60 GHz sounder for propagation channel measurements over short/medium distances," *IEEE Trans. Instrum. Meas.*, vol. 63, no. 2, pp. 343–351, Feb. 2014.
[27] M. J. Castelli, *LAN Switching First-Step*. Indianapolis, IN, USA: Cisco Press, 2004.
[28] D. A. Wassie, G. Berardinelli, F. M. L. Tavares, T. B. Sørensen, and P. Mogensen, "An experimental study of advanced receivers in a practical dense small cells network," in *Proc. 9th Int. Workshop Multiple Access Commun. (MACOM)*, Nov. 2016, pp. 3–14.
[29] O. Tonelli, "Experimental analysis and proof-of-concept of distributed mechanisms for local area wireless networks," Ph.D. dissertation, Dept. Electron. Syst., Univ. Aalborg, Aalborg, Denmark, 2014.
[30] Y. Wen, W. Huang, and Z. Zhang, "CAZAC sequence and its application in LTE random access," in *Proc. IEEE Inf. Theory Workshop (ITW)*, Mar. 2007, pp. 544–547.
[31] H. Holma, and A. Toskala, Eds., *LTE for UMTS: OFDMA and SC-FDMA Based Radio Access*. Hoboken, NJ, USA: Wiley, 2009.
[32] R. G. Lyons, *Understanding Digital Signal Processing*, 2nd ed. Englewood Cliffs, NJ, USA: Prentice-Hall, 2004.
[33] P. H. Moose, "A technique for orthogonal frequency division multiplexing frequency offset correction," *IEEE Trans. Commun.*, vol. 42, no. 10, pp. 2908–2914, Oct. 1994.
[34] J. H. Yooh and V. K. Wei, "On synchronizing and detecting multicarrier CDMA signals," in *Proc. 4th IEEE Int. Conf. Univ. Pers. Commun. (ICUPC)*, Nov. 1995, pp. 512–516.
[35] B. Yang, K. B. Letaief, R. S. Cheng, and Z. Cao, "Channel estimation for OFDM transmission in multipath fading channels based on parametric channel modeling," *IEEE Trans. Commun.*, vol. 49, no. 3, pp. 467–479, Mar. 2001.
[36] T. L. Hansen, B. H. Fleury, and B. D. Rao, "Superfast line spectral estimation," *IEEE Trans. Signal Process.*, vol. 66, no. 10, pp. 2511–2526, May 2018.
[37] Wanshih Electronic. *WSS007 Dual Band Antenna*. Accessed: Oct. 2018. [Online]. Available: http://www.wanshih.com.tw/products_3.php?sgid=2&gid=131
[38] *Guidelines for Evaluation of Radio Transmission Technologies for IMT-2000*, ITU-R Rec. M.1225-0, Feb. 1997.
[39] H. T. Friis, "A note on a simple transmission formula," *Proc. IRE*, vol. 34, no. 5, pp. 254–256, May 1946.
[40] D. A. Wassie, I. Rodriguez, G. Berardinelli, F. M. L. Tavares, T. B. Sorensen, and P. Mogensen, "Radio propagation analysis of industrial scenarios within the context of ultra-reliable communication," in *Proc. 87th Veh. Technol. Conf. (VTC-Spring)*, Jun. 2018, pp. 1–6.
[41] P. C. F. Eggers, M. Angjelichinoski, and P. Popovski, "Wireless channel modeling perspectives for ultra-reliable low latency communications," *IEEE Trans. Wireless Commun.*, to be published. Accessed: Oct. 2018. [Online]. Available: https://arxiv.org/abs/1705.01725v2

DEREJE ASSEFA WASSIE received the B.Sc. degree in electrical engineering from Jimma University, Ethiopia, in 2008, and the M.Sc. degree in telecommunication engineering from Aalborg University, Denmark, in 2011, where he is currently pursuing the Ph.D. degree in wireless communication with the Department of Electronic Systems. His main research interests include wireless communication system testbed design, enhanced mobile broadband communications, ultra-reliable communications, and the industrial Internet of Things.

IGNACIO RODRIGUEZ received the Telecommunication Engineering degree (B.Sc. + M.Sc.) from the University of Oviedo, Spain, and the M.Sc. degree in mobile communications and the Ph.D. degree in wireless communications from Aalborg University, Denmark. Since 2016, he has been a Postdoctoral Researcher with Aalborg University. He is currently an External Research Engineer with Nokia Bell Labs. His research interests include radio propagation, channel modeling, radio network planning and optimization, ultra-reliable and low-latency communications, and the industrial Internet of Things. He was a co-recipient of the IEEE VTS 2017 Neal Shepherd Memorial Best Propagation Paper Award.

GILBERTO BERARDINELLI received the first and second-level degrees *(cum laude)* in telecommunication engineering from the University of L'Aquila, Italy, in 2003 and 2005, respectively, and the Ph.D. degree from Aalborg University, Denmark, in 2010, where he is currently an Associate Professor with the Wireless Communication Networks Section. He is also in tight cooperation with Nokia Bell Labs. His research interests include physical layer, medium access control, and radio resource management design for the fifth-generation (5G) systems. He is currently part of the EU funded research project ONE5G that focuses on E2E-aware optimizations and advancements for the network edge of 5G New Radio.

FERNANDO M. L. TAVARES received the M.Sc. degree in wireless communications from the University of Brasilia, Brazil, in 2009, and the Ph.D. degree in wireless communications from Aalborg University, Denmark, in 2015. Since 2011, he has been a Visiting Researcher with Nokia Bell Labs, Denmark. He is currently an Assistant Professor in wireless communication networks with Aalborg University. His research interests include multiple input multiple output, interference management, and advanced transceiver design.

TROELS B. SØRENSEN received the M.Sc.E.E. degree, in 1990, and the Ph.D. degree in wireless communications from Aalborg University, in 2002. He was involved in the type approval test methods as part of ETSI standardization activities. Since 1997, he has been with Aalborg University, where he is currently an Associate Professor with the Section for Wireless Communication Networks. He has successfully supervised more than 15 Ph.D. students. He has published more than 120 journal and conference papers. His research and teaching activities include cellular network performance and evolution, radio resource management, propagation characterization, and related experimental activities.

THOMAS L. HANSEN received the M.Sc. degree *(cum laude)* in electrical engineering and the Ph.D. degree in wireless communication from Aalborg University, Denmark, in 2014 and 2018, respectively. In 2013 and 2015, he was a Visiting Scholar with the University of California, San Diego, USA. He is currently a Researcher and Developer with 3Shape, Denmark. His research interests include signal processing, machine learning, optimization, and wireless communication. He received the Best Student Paper Award (First Place) from the 2014 IEEE Sensor Array and Multichannel Signal Processing Workshop and the Award from IDA Efondet for his master's dissertation.

PREBEN MOGENSEN received the M.Sc. and Ph.D. degrees from Aalborg University, in 1988 and 1996, respectively. Since 1995, he has been part-time associated with Nokia. Since 2000, he has been a Full Professor with Aalborg University, where he is currently leading the Wireless Communication Networks Section, Department of Electronic Systems. He is also a Principal Engineer with Nokia Bell Labs. He has supervised over 35 successfully finalized Ph.D. candidates. He has co-authored over 300 papers in various domains of wireless communication. His current research interest includes fifth-generation and machine-type communication/the Internet of Things.